JPE 16-5-16

http://dx.doi.org/10.6113/JPE.2016.16.5.1773
ISSN(Print): 1598-2092 / ISSN(Online): 2093-4718

Wide Air-gap Control for Multi-module Permanent Magnet Linear Synchronous Motors without Magnetic Levitation Windings

Deok-Je Bang* and Seon-Hwan Hwang†

*Electric Motor Research Center, Electric Propulsion Research Division, Korea Electrotechnology Research Institute (KERI), Changwon, Korea
†Department of Electrical Engineering, Kyungnam University, Changwon, Korea

Abstract

This paper proposes a wide air-gap control method for the multi-module permanent magnet linear synchronous motor (MM-PMLSM) based on independent vector control. In particular, the MM-PMLSM consists of symmetrical multi-module and multi-phase structures, which are basically three-phase configurations without a neutral point, unlike conventional three-phase machines. In addition, there are no additional magnetic levitation windings to control the normal force of the air-gap between each stator and mover. Hence, in this paper, a *dq*-axis current control applying a *d-q* transformation and an independent vector control are proposed for the air-gap control between the two symmetric stators and mover of the MM-PMLSM. The characteristics and control performance of the MM-PMLSM are analyzed under the concept of vector control. As a result, the proposed method is easily implemented without additional windings to control the air-gap and the mover position. The effectiveness of the proposed independent vector control algorithm is verified through experimental results.

Key words: D-axis control, Independent vector control, MM-PMLSM, Position control, Wide air-gap control

I. INTRODUCTION

Permanent magnet (PM) linear synchronous motors are beginning to have widespread industrial applications in transportation systems, automation systems, and machine tool positioning. The main features of PM linear synchronous motors are the high force density achievable and the high positioning precision and accuracy associated with the mechanical system's simplicity [1]-[3]. The permanent magnet linear synchronous motors (PMLSMs) with a multi-module and a wide air-gap described in this paper have not been widely used in industrial applications. Therefore, several control algorithm can be applied for improving the performance of these machines [4]-[6].

In particular, linear motor drives need to develop not only a contactless levitation system but also a contact-free propulsion system to drive the transportation systems. Generally, linear motors produce a high normal force when compared to the thrust force developed by the motor itself [2], [3]. In addition, the use of a magnetic levitation system is steadily increasing in high-speed motor drives, generators with a flywheel drive, medical equipment, and in harsh environments such as low temperature, high temperature, and vacuum due to the characteristics of high velocity, no wear, and no maintenance. However, magnetic levitation systems needs additional windings to produce the suspension force of rotating machines [7]-[9].

However, in this paper there are no additional windings to generate the normal force that controls the air-gap separately from conventional systems. It has advantages in terrms of reducing several problems such as large, heavy, and complex conventional structures for air-gap control [10], [11]. In addition, this paper focuses on the continuous air-gap and position controls in the special structures of the developed MM-PMLSM [4], [12]-[14].

An independent vector control applying a transformation matrix and a symmetric three-phase configuration produce

Manuscript received Jan. 13, 2016; accepted May 13, 2016
Recommended for publication by Associate Editor Gaolin Wang.
†Corresponding Author: seonhwan@kyungnam.ac.kr
Tel: +82-55-249-2744, Fax: +82-505-999-2161, Kyungnam University
*Electric Motor Research Center, Electric Propulsion Research Center, KERI, Korea

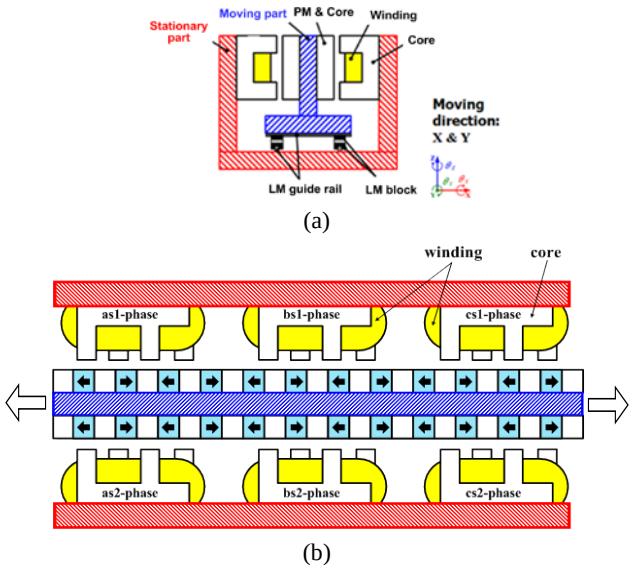

Fig. 1. Structures of MM-PMLSM. (a) Front view. (b) Upper view.

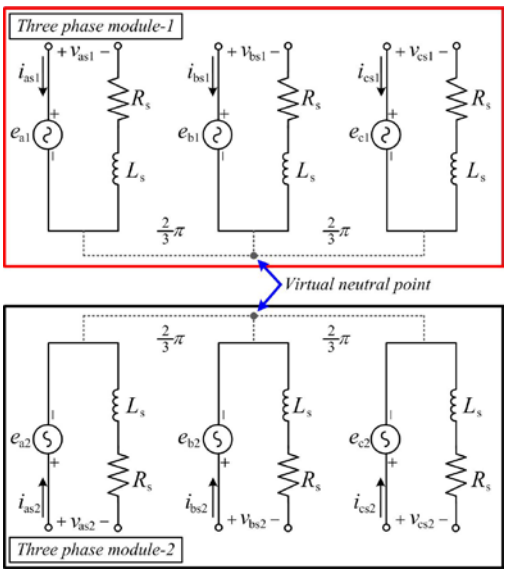

Fig. 2. Three-phase equivalent circuits of MM-PMLSM.

the thrust and normal forces of the MM-PMLSM. The control performance and characteristics of the proposed air-gap and position control algorithms are analyzed with mathematical modeling. The proposed method is easily implemented by using the vector control concept and less computational efforts. Finally, the feasibility and effectiveness of the proposed drive system are verified through several experiments.

II. Modeling of MM-PMLSLM

A. Configuration of MM-PMLSM

Fig. 1 shows the structure of the MM-PMLSM. From Fig. 1 (a), it can be seen that the MM-PMLSM drive system has the moving and stationary parts to realize levitation and propulsion by controlling the normal force and thrust force [15]-[17]. The LM guide rail only supports the weight of the mover of the MM-PMLSM. In addition, the MM-PMLSM consists of symmetrical independent single-phase windings based on three-phase winding with two sets, which are installed on the left and right sides of its mover as shown in Fig. 1(b). Each stator phase winding is separated by 120° electrical degrees [4], [5]. There are no additional windings to produce the normal force related to magnetic levitation, unlike conventional systems. Finally, only the coils facing the mover PMs control the air-gap length and mover position of the MM-PMLSM.

B. Mathematical Model

Fig. 2 shows three-phase equivalent circuits of the MM-PMLSM. As shown in Fig. 2, each three-phase module has a virtual neutral point because of the multi-module configuration. When considering only the red dashed line in Fig. 2, each phase voltage equation can be expressed as:

$$v_j = R_s i_j + \frac{d\lambda_j}{dt}, \quad j = as1, bs1, cs1 \tag{1}$$

where v_j is the stator voltage in each phase. R_S is the stator resistance. i_j and λ_j are the stator current and flux linkage, respectively.

From (1), the flux linkage caused by the PM can be derived as follows:

$$\lambda_j = L_{jk} i_j + \lambda_{jf}, \quad j = as1, bs1, cs1 \tag{2}$$

where λ_{jf} is the j-phase flux linkage according to the PM.

In (2), if the *j*-and *k*-phases are the same, L_{jk} can be expressed as the self-inductance between the j-phase and the k-phase L_S. On the contrary, if the *j*-phase and the *k*-phase are different, L_{jk} is the mutual inductance between the j-phase and the k-phase.

Through (1) and (2), each single-phase voltage equation can be rewritten as follows [14]:

$$\begin{aligned} v_j &= R_s i_j + \frac{d\lambda_j}{dt} \\ &= R_s i_j + \frac{d}{dt}(L_{jj} i_j + \lambda_{if}) \\ &= R_s i_j + \frac{dL_s}{dt} i_j + L_s \frac{di_j}{dt} + \frac{d\lambda_{jf}}{dt} \end{aligned} \tag{3}$$

The self-inductance, L_S, and flux linkage caused by the mover permanent magnet, λ_{jf}, depend on the air-gap length, phase current and mover displacement as given by:

$$\frac{dL_s}{dt} = \frac{\partial L_s}{\partial x}\frac{dx}{dt} + \frac{\partial L_s}{\partial i_j}\frac{di_j}{dt} + \frac{\partial L_s}{\partial y}\frac{dy}{dt} \tag{4}$$

$$\frac{d\lambda_{jf}}{dt} = \frac{\partial \lambda_{jf}}{\partial x}\frac{dx}{dt} + \frac{\partial \lambda_{jf}}{\partial i_j}\frac{di_j}{dt} + \frac{\partial \lambda_{jf}}{\partial y}\frac{dy}{dt} \tag{5}$$

where *x* is the displacement of the air-gap length, and *y* is the mover position.

After consideration of Eqs. (4) and (5), the voltage equation is represented by:

$$v_j = R_s i_j + \left(L_s + \frac{\partial L_s}{\partial i_j} i_j + \frac{\partial \lambda_{jf}}{\partial i_j} \right) \frac{di_j}{dt} + \left(\frac{\partial L_s}{\partial x} i_j + \frac{\partial \lambda_{jf}}{\partial x} \right) \frac{dx}{dt} + \left(\frac{\partial L_s}{\partial y} i_j + \frac{\partial \lambda_{jf}}{\partial y} \right) \frac{dy}{dt} \quad (6)$$

In general cases, the air-gap displacement is zero and a saturation effect does not appear. As a result, a simplified voltage equation per phase can be calculated as follows:

$$v_j = R_s i_j + L_s \frac{di_j}{dt} + K_f v_r \quad (7)$$

where $K_f = \left(\frac{\partial L_s}{\partial y} i_j + \frac{\partial \lambda_f}{\partial y} \right)$, $L_s = L_s + \frac{\partial L_s}{\partial i_j} i_j + \frac{\partial \lambda_{if}}{\partial i_j}$ and $v_r = \frac{dy}{dt}$.

In addition, the mutual inductance between each phase winding can be considered zero due to the independent magnetic circuit of each phase [4], [5]. Therefore, the *dq*-axis voltage equations, considering the mutual inductance in the synchronous reference frame, can be represented by:

$$\begin{aligned} v_{ds1}^e &= R_s i_{ds1}^e + L_{ds1} \frac{di_{ds1}^e}{dt} - \frac{\pi}{\tau} v_r L_{qs1} i_{qs1}^e \\ v_{qs1}^e &= R_s i_{qs1}^e + L_{qs1} \frac{di_{qs1}^e}{dt} - \frac{\pi}{\tau} v_r L_{ds1} i_{ds1}^e + \frac{\pi}{\tau} v_r \lambda_{PM} \end{aligned} \quad (8)$$

The *dq*-axis linkages in the synchronous reference frame can be derived as:

$$\begin{aligned} \lambda_{ds1}^e &= L_{ds1} i_{ds1}^e + \lambda_{PM} \\ \lambda_{qs1}^e &= L_{qs1} i_{qs1}^e \end{aligned} \quad (9)$$

From (8) to (9), the magnetic co-energy, W', in the air-gap can be calculated as:

$$\begin{aligned} W' &= \frac{1}{2} (\lambda_{PM} + \lambda_{ds1}^e i_{ds1}^e + \lambda_{qs1}^e i_{qs1}^e) \\ &= \frac{1}{2} \left\{ \lambda_{PM} + \lambda_{PM} i_{ds1}^e + L_{ds1} {i_{ds1}^e}^2 + L_{qs1} {i_{qs1}^e}^2 \right\} \end{aligned} \quad (10)$$

$$W' = \frac{1}{2} \left\{ \lambda_{PM} + \lambda_{PM} i_{ds1}^e + \left(\frac{L_{d0}}{g} + L_{ls} \right) {i_{ds1}^e}^2 + \left(\frac{L_{q0}}{g} + L_{ls} \right) {i_{qs1}^e}^2 \right\} \quad (11)$$

Therefore, the normal force, F_X, can be received by the derivative of the magnetic co-energy according to the axial displacement as:

$$F_{x1} = \frac{\partial W'}{\partial x} = -\frac{1}{2} \frac{L_{d0}}{g^2} \frac{dg}{dx} {i_{ds1}^e}^2 - \frac{1}{2} \frac{L_{d0}}{g^2} \frac{dg}{dx} {i_{qs1}^e}^2 \quad (12)$$

Furthermore, the thrust force, F_y, generated by the independent three-phase stator is as follows:

$$\begin{aligned} F_{y1} &= \frac{3}{2} \frac{\pi}{\tau} (\lambda_{ds1}^e i_{qs1}^e - \lambda_{qs1}^e i_{ds1}^e) \\ &= \frac{3}{2} \frac{\pi}{\tau} (\lambda_{PM} i_{qs1}^e + (L_{ds1} - L_{qs1}) i_{ds1}^e i_{qs1}^e) \\ &= \frac{3}{2} \frac{\pi}{\tau} \lambda_{PM} i_{qs1}^e + \frac{3}{2} \frac{\pi}{\tau} \frac{(L_{d0} - L_{q0})}{g} i_{ds1}^e i_{qs1}^e \end{aligned} \quad (13)$$

In (13), the first term is the magnetic force caused by the mover PM and the *q*-axis current. The second is the reluctance force from the difference between the *d*-axis and *q*-axis inductances.

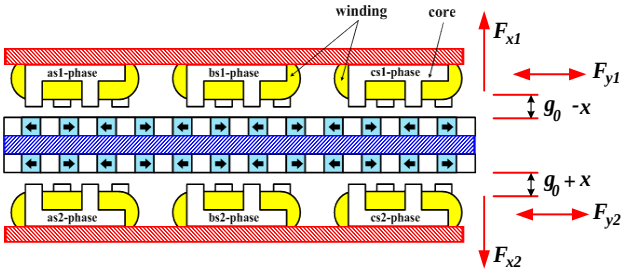

Fig. 3. Thrust and normal forces in the MM-PMLSM.

From the above equations, the total normal force, F_{normal}, to control the air-gap can be calculated by:

$$\begin{aligned} F_{normal} &= F_{x1} - F_{x2} \\ &= -\frac{L_{d0}}{2(g_0 - x)^2} {i_{ds1}^e}^2 - \frac{L_{q0}}{2(g_0 - x)^2} {i_{qs1}^e}^2 \\ &\quad - \frac{L_{d0}}{2(g_0 - x)^2} {i_{ds2}^e}^2 - \frac{L_{q0}}{2(g_0 - x)^2} {i_{qs2}^e}^2 \end{aligned} \quad (14)$$

where g_0 is the equilibrium point.

Through (13), the total thrust force, F_{thrust}, can be obtained as follows:

$$\begin{aligned} F_{thrust} &= F_{y1} + F_{y2} \\ &= \frac{3}{2} \frac{\pi}{\tau} \lambda_{PM} i_{qs1}^e + \frac{3}{2} \frac{\pi}{\tau} \frac{(L_{d0} - L_{q0})}{(g_0 - x)^2} i_{ds1}^e i_{qs1}^e \\ &\quad + \frac{3}{2} \frac{\pi}{\tau} \lambda_{PM} i_{qs2}^e + \frac{3}{2} \frac{\pi}{\tau} \frac{(L_{d0} - L_{q0})}{(g_0 - x)^2} i_{ds2}^e i_{qs2}^e \end{aligned} \quad (15)$$

In (14) and (15), to linearize the equilibrium point ($x = 0$), the normal and thrust forces can be derived as:

$$\begin{aligned} F_{normal} &= F_{x1} - F_{x2} \\ &= \frac{L_{d0}}{2g_0^2} \left({i_{ds2}^e}^2 - {i_{ds1}^e}^2 \right) + \frac{L_{q0}}{2g_0^2} \left({i_{qs2}^e}^2 - {i_{qs1}^e}^2 \right) \end{aligned} \quad (16)$$

$$\begin{aligned} F_{thrust} &= F_{y1} + F_{y2} \\ &= \frac{3}{2} \frac{\pi}{\tau} \lambda_{PM} (i_{qs1}^e - i_{qs2}^e) + \frac{3}{2} \frac{\pi}{\tau} \frac{(L_{d0} - L_{q0})}{g_0} (i_{ds1}^e i_{qs1}^e + i_{ds2}^e i_{qs2}^e) \end{aligned} \quad (17)$$

In (16), the first component is the normal force, which is controlled by the *d*-axis current of each independent three-phase. In addition, the *q*-axis current influences the normal force of the MM-PMLSM. The first term in (17) represents the thrust force and the second term is the reluctance force caused by the *dq*-axis currents of each stator. By assuming that the synchronous frame *d*-axis current is the same on each side, the reluctance force is eliminated.

Fig. 3 shows the thrust and normal forces in the *X*-axis and *Y*-axis directions in the two axis coordinates. While the direction of each normal force is opposing, the thrust forces have the same direction.

III. Independent Vector Control for the MM-PMLSM

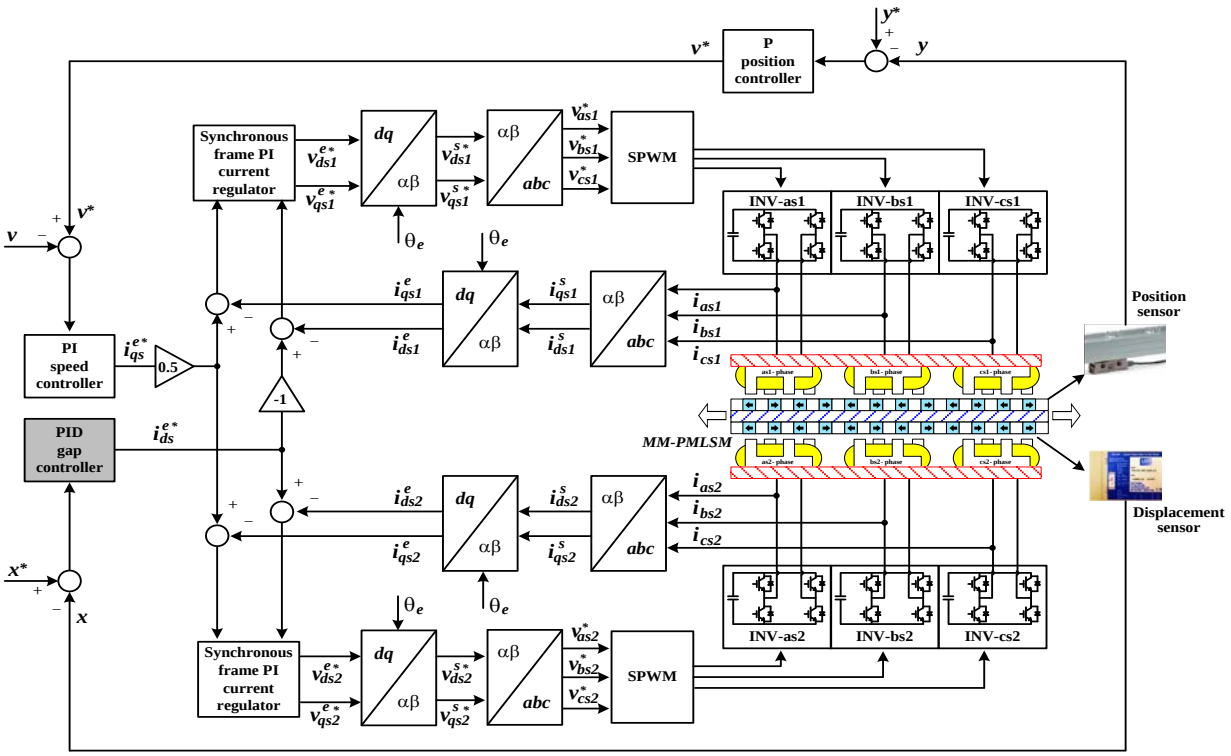

Fig. 4. Overall control block diagram of independent vector control for MM-PMLSM.

From the mathematical modeling of the normal and thrust forces, the independent vector control concept can be applied to control the MM-PMLSM. Therefore, in order to control the air-gap between the stator and the mover, the normal force is the focus of this paper. The normal force related to the air-gap variation is regulated to levitate the mover of the MM-PMLSM. The unbalanced flux density in each air-gap causes an unbalanced normal force. Namely, the field weakening control is operated and the air-gap flux density is decreased. As a result, the air-gap length is increased [7]-[9]. Finally, the air-gap can be adjusted in an arbitrary direction by controlling the *d*-axis current in the vector control strategy.

Fig. 4 shows a block diagram of the independent vector control for the MM-PMLSM. In order to take advantage of the modular structure three-phase sets, H-bridge modular inverters are used to control the air-gap length and the mover position of the MM-PMLSM drive system. Namely, each module is driven by a separate inverter module forming an independent drive unit.

The air-gap information from the displacement sensor is calculated to the *d*-axis current command through a PID gap controller. The thrust force for tracking the mover position control is produced by position and speed controllers as shown in Fig. 4. Each phase current is transformed into the *d-q* rotating frame by the transformation matrix.

The independent vector control of the MM-PMLSM is operated through two components, which are the normal force-producing current i_{ds}^{e} and the thrust force-producing current i_{qs}^{e}. The thrust force of the MM-PMLSM can be controlled by the *q*-axis current, while the normal force can be controlled by the *d*-axis current.

IV. Experiments

Fig. 5 shows an overall block diagram of the MM-PMLSM drive system to verify the proposed control algorithm. As shown in this figure, the MM-PMLSM used in the experiments is based on a symmetric configuration with the independent three-phases. In addition, single-phase bi-directional AC/DC/AC converter modules are implemented by IGBT modules with a switching frequency of 10kHz.

The entire control algorithm is executed by a digital signal processor (DSP) control system. A displacement sensor for controlling the air-gap is installed at the stationary part. Detailed specifications of the MM-PMLSM are shown in Table I.

Fig. 6 depicts a photo of the actual MM-PMLSM, which includes six single-phase power converters, a control board, and a displacement sensor.

In order to drive the air-gap control and the position control simultaneously, the independent three-phase windings and the proposed vector control algorithm are used without any additional windings to control the air-gap length.

Fig. 7 shows experimental result of the independent vector control for the MM-PMLSM when the air-gap command is

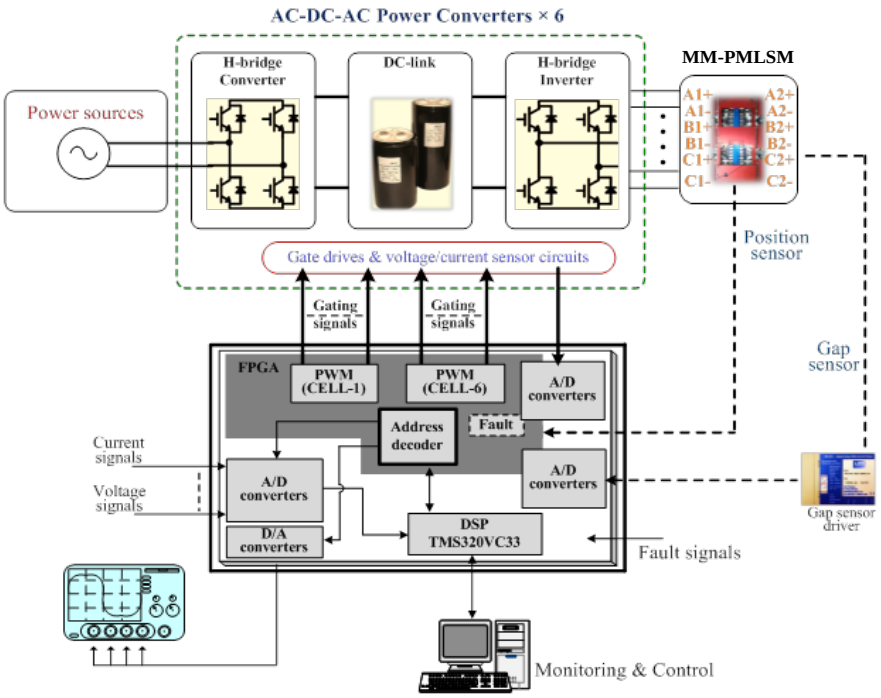

Fig. 5. Block diagram of MM-PMLSM.

TABLE I
SPECIFICATIONS OF THE MM-PMLSM

	Parameters	Values	Unit
Rated MM-PMLSM	MMF	6,000	[AT]
	Thrust force	250	[N], Per phase
Mover PM	Material	Ferrite	
	Thickness	8	[mm]
Stator	Material	S20c	
	Pole pitch	20	[mm]
	Thickness	16	[mm]
	Width	30	[mm]
	Height	80	[mm]
Mover	Material	S20c	
	Width	110	[mm]
	Height	35	[mm]

changed from 1.2 [mm] to 3.0 [mm] and the mover position varies from 0.06 [m] to 0.1 [m]. The air-gap and position commands are given after 10 [s]. The actual mover position and air-gap track each command as shown in Fig. 7. In a linear motor system, the air-gap control should be operated with the position control. If not, the position of the mover is not fixed according to the air-gap control.

Fig. 8 describes experimental results of the effects of the *d*-axis current variation on the thrust force. The air-gap is changed from 2.5 [mm] to 4.5 [mm]. Despite the variation of the air-gap, the real mover position does not change after the position control is operated.

Fig. 9 shows experimental waveforms under air-gap command variations while the mover position is constant. In spite of an air-gap command variation from 2.5 [mm] to 4.0 [mm], the actual air-gap is well controlled by the

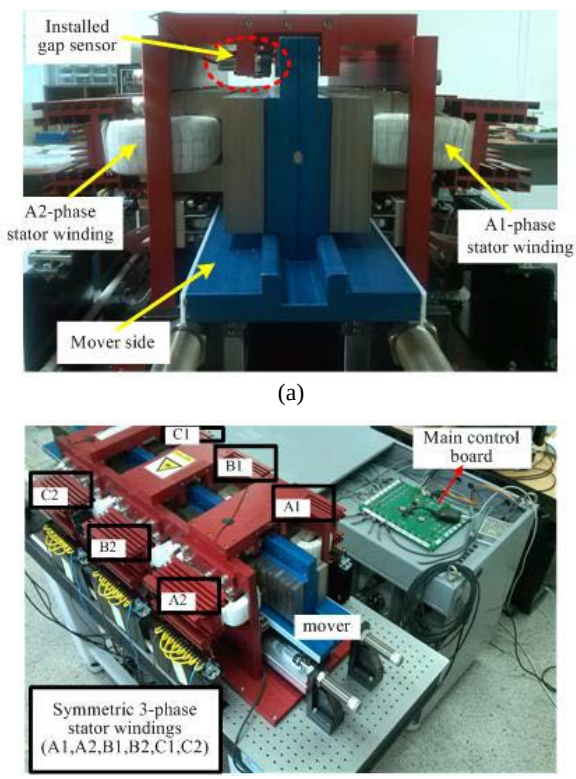

Fig. 6. Pictures of MM-PMLSM drive system. (a) Front view. (b) Upper view.

proposed independent vector control with the *d-q* transformation. According to the waveform, an air-gap of 4 [mm] is almost the equilibrium point in this system and the *dq*-axis currents are zero. In contrast, in the other position of

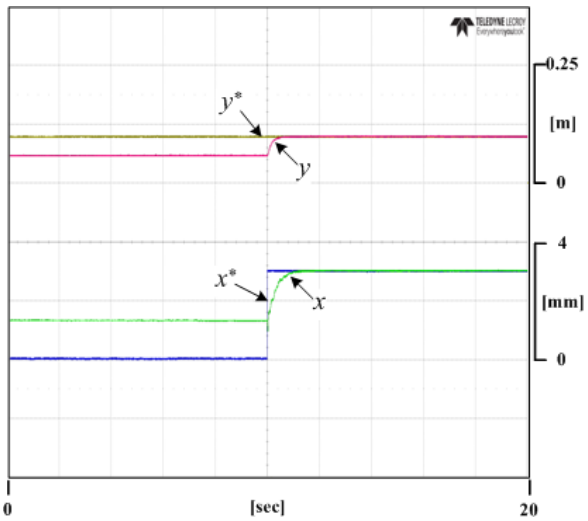

Fig. 7. Experimental waveform according to simultaneous mover position and air-gap command changes.

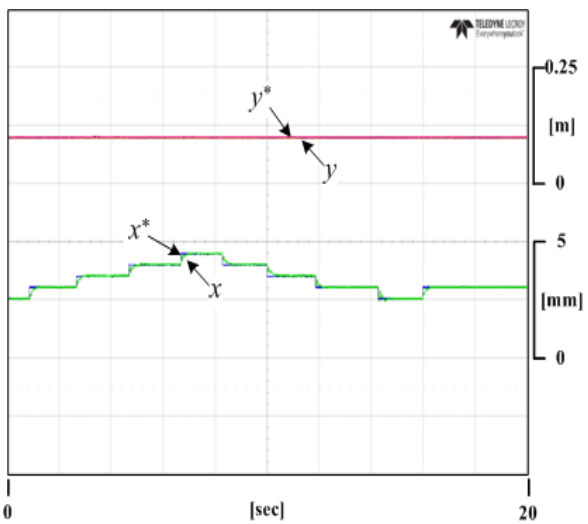

Fig. 8. Experimental waveform of air-gap control during standstill.

the air-gap, the *dq*-axis currents have different directions and the same magnitude values.

In Fig. 10, the *dq*-axis currents are shown while the air-gap command is changed. When the mover position is constant, the effect of the air-gap variation on the *q*-axis current is not generated. The separated windings due to the multi-module structure have no coupling flux effects between each other.

From Fig. 7 to Fig. 10, the mover stroke is constant. The total steady-state errors are less than about 14[um].

Fig. 11 presents a waveform under the constant air-gap command while the mover stroke oscillates from 0.05 [m] to 0.2 [m]. Nevertheless, when the mover stroke changes, the air-gap is nearly constant at 3 [mm] under the maximum and minimum target positions. However, while accelerating the section, the air-gap variation is below 78 [um].

Fig. 12 shows an experimental waveform when the mover position is changed from 0.05 [m] to 0.2 [m] and the air-gap command changes from 3.0 [mm] to 4.5 [mm]. From Fig. 12,

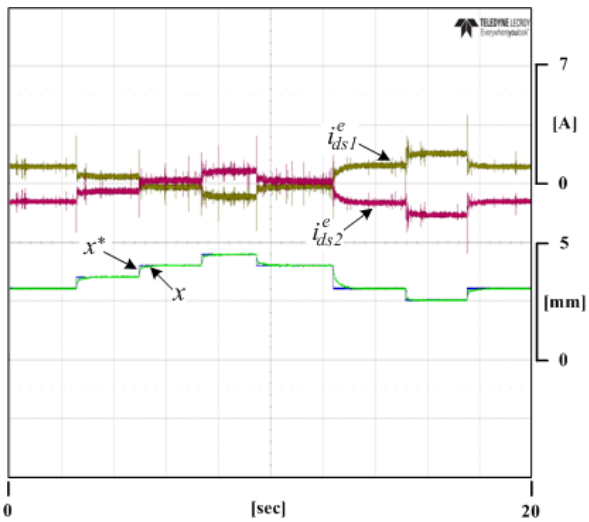

Fig. 9. Experimental waveform of air-gap control under the air-gap command variation.

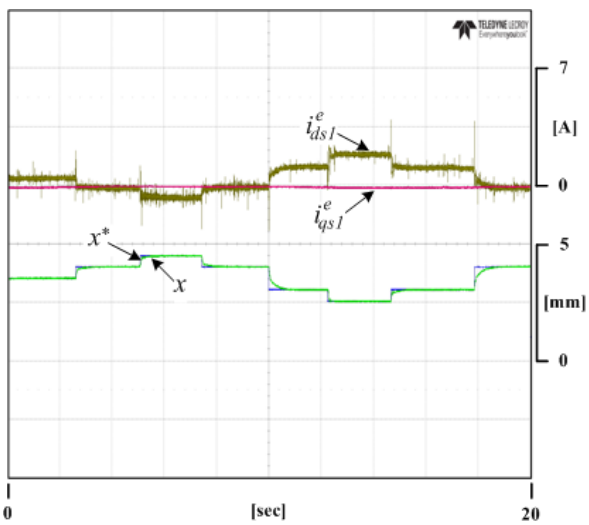

Fig. 10. Experimental waveform of each a-phase current at constant mover stroke operations.

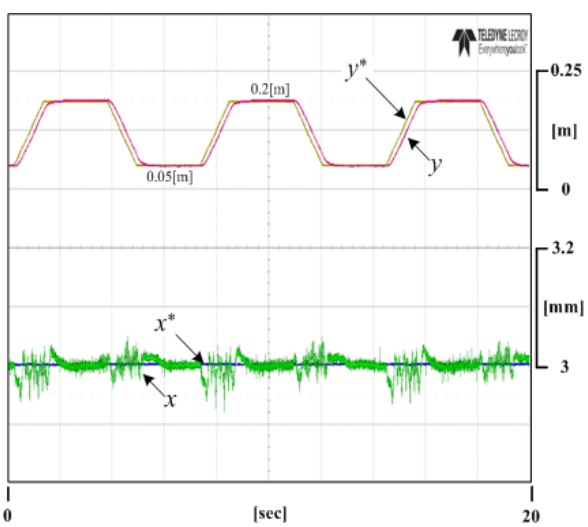

Fig. 11. Experimental waveform of constant air-gap command at constant mover stroke operations.

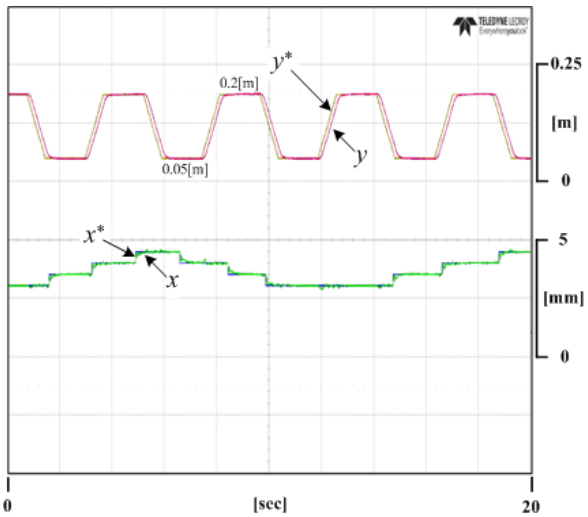

Fig. 12. Experimental waveform of various air-gap commands during constant mover stroke operations.

the air-gap and position control operate well simultaneously.

In Fig. 11 and Fig. 12, the actual position response according to the position command is slow because the normal force depends on the thrust force, which is increased in order to improve the transient response times of the position control. Namely, the air-gap variation is directly generated by the thrust force from the movement of the mover.

V. CONCLUSIONS

In this paper, air-gap and position control methods based on independent vector control for a developed MM-PMLSM without additional magnetic levitation windings are proposed. In addition, mathematical modeling for the normal and thrust force is analyzed in detail.

According to the structural characteristics, the displacement of the air-gap between the mover and the stators is controlled by the *d*-axis current, and the mover position is adjusted by the *q*-axis current under independent vector control. As a result, air-gap and position control based on multi-phase and multiple-module structures can be easily implemented by using the proposed independent vector control while having a reduced computational burden. In addition, it is possible to facilitate the system extension of the MM-PMLSM with multiple-modules. The usefulness of the proposed vector control method was verified through experimental results in this paper.

ACKNOWLEDGMENT

This work was supported by the Korea Electro technology Research Institute grant funded by the Korea government (15-12-N0101-18), Basic Science Research Program through the National Research Foundation of Korea (NRF) funded by the Ministry of Education, Science and Technology (No.2013R1A1A1013670), and National IT Promotion Agency (S0170-15-1078).

REFERENCES

[1] D. H. Kang, "A study on the design of transverse flux linear motor with high power density," *IEEE International Symposium on*, Vol. 2, pp. 707-711, 2002.

[2] W. Y. Kim, J. M. Lee, and S. J. Kim, "Rolling motion control of a levitated mover in a permanent-magnet-type bearingless linear motor," *IEEE Trans. Magn.*, Vol. 46, No. 6, pp. 2482-2485, Jun. 2010.

[3] W. G. Kim and S. J. Cho, "Control of transverse flux linear motor to the linear and curve section by using low-cost position sensors," *Industrial Electronics, 2007. ISIE 2007 IEEE International Symposium on*, pp. 1322-1326, Nov. 2007.

[4] S. H. Hwang, H. Li, J. W. Park, J. M. Kim, and D. J. Bang, "Vector control of multiple-module transverse flux PM generator for large-scale direct-drive wind turbines," 2011 *IEEE, Energy Conversion Congress and Exposition*, pp. 2365-2372, 2011.

[5] D. Bang, H. Polinder, J. A. Ferreira, and S. S. Hong, "Structural mass minimization of large direct-drive wind generators using a buoyant rotor structure," *Energy Conversion Congress and Exposition, 2010 IEEE*, pp. 3561-3568, 2010.

[6] O. S. Park, J. W. Park, C. B. Bae, and J. M. Kim, "A dead time compensation algorithm of independent multi-phase PMSM with three-dimensional space vector control," *Journal of Power Electronics*, Vol. 13, No. 1, pp. 77-85, Jan. 2013.

[7] S. Kobayashi, M. Ooshima, and M. Nasir Uddin, "A radial position control method of bearingless motor based on *d-q* axis current control," *IAS, 2011 IEEE*, pp. 1-8, 2011.

[8] M. Ooshima, S. Kobayashi, and M. Nasir Uddin, "Magnetic levitation tests of a bearingless motor based on *d-q* axis current control," *IAS, 2012 IEEE*, pp. 1-7, 2012.

[9] Z. Guan, D. H. Lee, J. W. Ahn, and F. Zhang, "A compensation strategy of suspending force in hybrid type stator pole bearingless switched reluctance motor," *ICEMS, 2011 International Conference on*, pp. 1-6, 2011.

[10] S. H. Hwang, D. J. Bang and J. W. Kim, "Air gap control of multi-phase transverse flux permanent magnet linear synchronous motor by using independent vector control," in *International Power Electronics Conference(IPEC 2014)*, pp. 2427-2432, 2014.

[11] T. D. Nhuyen, G. F. H. Beng, K. J. Tseng, D. M. Vilathgamuwa and X. Zhang, "Modeling and position-sensorless control of a dual-airgap axial flux permanent magnet machine for flywheel energy storage systems," *Journal of Power Electronics*, Vol. 12, No. 5, pp. 758-768, Sep. 2012.

[12] Q. D. Nhuyen and S. Ueno, "Modeling and control of salient-pole permanent magnet axial-gap self-bearing motor," *IEEE/ASME Trans. Mechatron.*, Vol. 16, No. 3, pp. 518-526, Jun. 2011.

[13] H. Wang, D. H. Lee, and J. W. Ahn, "Radial force control of a novel hybrid pole BLLSRM," *Journal of Power Electronics*, Vol. 9, No. 6, pp. 845-853, Nov. 2009.

[14] S. Ueno and Y. Okada, "Vector control of an induction type axial gap combined motor-bearing," in *Proc. IEEE Int.*

Conf. Adv. Intell. Mechatronics, Atlanta, GA, pp. 794-799, 1999.
[15] S. Zhang and F. L. Luo, "Direct control of radial displacement for bearingless permanent-magnet-type synchronous motors," *IEEE Trans. Ind. Elec.*, Vol. 56, No. 2, pp. 542-552, Feb. 2009.
[16] S. H. Hwang, S. K. Kwon, Y. G. Hwang and D. J. Bang, "Coordinated control of an independent multi-phase permanent magnet-type transverse flux linear machine based on magnetic levitation," *Journal of KIIEE*, Vol. 28, No. 12, pp.95-102, Dec. 2014.
[17] C. N. Heo, B. G. Jeong, S. H. Hwang and D. J. Bang, "Double-sided air gap control of module-based permanent magnet synchronous machine for low-speed and high-torque applications," *ICPE-ECCE Asia, 2015 9th International Conference on*, pp. 1603-1608, 2015.

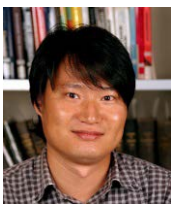

Deok-Je Bang received his B.S. and M.S. degrees in Mechanical Engineering from Pukyong National University, Busan, Korea, in 1996 and 1998, respectively. He received his Ph.D. degree in Electrical Engineering from the Delft University of Technology, Delft, Netherlands, in 2010. From 1998 to 2006, he worked as a Researcher in the area of electrical machines and automatic transportation systems. In 2011, he was a Principal Researcher and a Team Leader at the Wind Turbine Research Division, Hyundai Heavy Industries, Korea. Since 2012, he has been with the Electric Motor Research Center, Electric Propulsion Research Division, Korea Electrotechnology Research Institute (KERI), Changwon, Korea. His current research interests include direct-drive generator systems for renewable energy.

Seon-Hwan Hwang received his B.S., M.S., and Ph.D. degrees in Electrical Engineering from Pusan National University, Busan, Korea, in 2004, 2006, and 2011, respectively. From 2011 to 2012, he was with the Center for Advanced Power Systems (CAPS), Florida State University, Tallahassee, FL, USA. In 2012, he joined the Department of Electrical Engineering, Kyungnam University, Changwon, Korea. His current research interests include the control of electrical machines, power electronics, and wind power generation systems.